Extremophiles (2001) 5:303–311
Digital Object Identifier (DOI) 10.1007/s007920100206

ORIGINAL PAPER

Pedro Lamosa · Lorraine Brennan · Hans Vis
David L. Turner · Helena Santos

NMR structure of *Desulfovibrio gigas* rubredoxin: a model for studying protein stabilization by compatible solutes

Received: January 31, 2001 / Accepted: April 4, 2001 / Published online: August 17, 2001

Abstract Rubredoxins are small, soluble proteins that display a wide variation in thermostability, despite having a high degree of sequence similarity. They also vary in the extent to which they are stabilized by solutes such as diglycerol phosphate. Hence, they provide excellent models for studying the mechanisms of thermostabilization. Nuclear magnetic resonance (NMR) spectroscopy can be used to investigate interactions between molecules, as well as subtle changes in conformation in solution, and also provides a means to measure protein stability. The assignment of the proton NMR spectrum of the zinc rubredoxin from *Desulfovibrio gigas* is presented, together with its structure in solution. The stabilizing effect of diglycerol phosphate on rubredoxin is demonstrated and assessed by determining selected amide proton exchange rates; diglycerol phosphate at 100 mM concentration caused an additional structural stabilization of 1.2 ± 0.4 kJ/mol. The pattern of effects on the exchange rates is discussed in relation to the protein structure.

Key words Compatible solute · Rubredoxin · Protein stabilization · Amide proton exchange · NMR

Communicated by G. Antranikian

P. Lamosa · L. Brennan · H. Vis · D.L. Turner · H. Santos (✉)
Instituto de Tecnologia Química e Biológica, Universidade Nova de Lisboa, Rua da Quinta Grande 6, Apartado 127, 2780 Oeiras, Portugal
Tel. +35-12-14469828; Fax +35-12-14428766
e-mail: santos@itqb.unl.pt

D.L. Turner
Department of Chemistry, University of Southampton, Southampton, UK

Presented at the Third International Congress on Extremophiles, Hamburg, 2000

Introduction

Life at high temperatures requires both metabolic as well as structural adaptations. Among these, the thermostability of proteins strikes us as the most tantalizing. Although a wealth of data has been accumulated in recent years, we are still far from understanding the general rules that determine protein thermostability and, therefore, the ways in which stability could be improved through protein engineering (Jaenicke 1991; Jaenicke and Bohm 1998; Richards 1997).

The available knowledge, largely derived from comparative studies of the three-dimensional (3-D) structures of homologous proteins from microorganisms with very different optimal growth temperatures, has pointed to several structural features that seemed to correlate with a higher thermostability. Among these, salt-bridge networks, optimal packing of hydrophobic cores, decrease in surface loop lengths, and stabilization of secondary structure (e.g., terminal helix capping) have been suggested (Britton et al. 1995, 1999; Hensel 1993; Ladenstein and Antranikian 1998; Strop and Mayo 2000). However, as more data are gathered, several inconsistencies and limitations to the applicability of these explanations have become apparent (Karshikoff and Ladenstein 1998; Lebbink et al. 1999). Moreover, point mutations in amino acids that apparently do not fit any of these stabilizing strategies have proven to be crucial to thermostability (Perl et al. 2000).

Improved protein stability may also be achieved by extrinsic factors, such as compatible solutes (da Costa et al. 1998; Santos and da Costa 2001). In fact, some proteins of thermophilic origin, usually more stable than their mesophilic counterparts, show an unexpectedly low intrinsic thermostability in vitro (Hensel 1993), an observation that underlines the need for extrinsic stabilization in vivo. The beneficial effects of different compatible solutes on protein stability in vitro are well documented (Felix et al. 1999; Hensel and König 1988; Lamosa et al. 2000; Lippert and Galinski 1992; Ramos et al. 1997; Santoro et al. 1992; Scholz et al. 1992; Shima et al. 1998). However, the mechanisms responsible for this stabilization are not fully understood. According to the preferential exclusion model (Arakawa

and Timasheff 1985; Timasheff 1993), stabilizing molecules would make denaturation entropically less favorable by being excluded from the solvent–protein interface, but the correlation between exclusion factors and stability enhancement is not general (Arakawa et al. 1990). In fact, it seems that the magnitude of the stabilizing effect rendered by a given solute depends closely on the particular protein examined (Lamosa et al. 2000; Lippert and Galinski 1992), suggesting the involvement of specific solute–protein interactions.

Recently, we have examined rubredoxins from different sources for their thermostability in the presence or absence of diglycerol phosphate (DGP) (Lamosa et al. 2000), a solute identified in the hyperthermophile *Archaeoglobus fulgidus*, where it accumulates in response to salt stress (Martins et al. 1997). Although this solute appears to act as a general thermostabilizer of protein structure, we found that the presence of DGP stabilized the three homologous rubredoxins to different extents despite their high structural homology (Lamosa et al. 2000). There was no significant protective effect on one of the proteins whereas the others were highly stabilized. Understanding the molecular mechanisms underlying the protective effect of DGP on the structure of rubredoxins may reveal the general features of protein stabilization and possible direct solute–protein interactions.

Rubredoxins are ideally suited for investigating these mechanisms because they are highly homologous and well-characterized proteins (Sieker et al. 1994). Furthermore, they are small, which allows us to take advantage of the unique features of nuclear magnetic resonance (NMR) spectroscopy to characterize protein–solute interactions in detail and probe effects on protein dynamics. With this goal in mind, the gene encoding *Desulfovibrio gigas* rubredoxin was cloned and expressed in *Escherichia coli* (Lamosa et al. 2000) to provide protein in quantity and access to mutants for future studies. As the presence of the paramagnetic iron center causes considerable broadening of the signals of protons in its vicinity, the diamagnetic zinc form was used in this study. The assignment of the proton NMR spectrum of the zinc rubredoxin from *D. gigas* is presented here, together with its structure in solution. Furthermore, the changes in the $^{1}H/^{2}H$ amide exchange rate on addition of diglycerol phosphate were measured and are discussed in relation to structure stabilization.

Materials and methods

Sample preparation

Zinc-rubredoxin from *D. gigas* and diglycerol phosphate were obtained as previously described (Lamosa et al. 2000). Approximately 10 mg of rubredoxin was obtained and its purity assessed by native polyacrylamide gel electrophoresis (PAGE). The protein was concentrated and the buffer removed by ultrafiltration using a YM3 membrane (Amicon, Bedford, MA, USA). The final volume was 600 µl with a concentration of approximately 2.5 mM in 10% D_2O. The pH of the sample was adjusted to 7.6 with NaOH (0.1 M) or HCl (0.1 M).

NMR spectroscopy

^{1}H-NMR spectra were acquired on a Bruker DRX500 (Bruker, Rheinstetten, Germany) spectrometer. Assignments were obtained from spectra recorded at 308 K and pH 7.6; additional spectra were recorded at 300 K and 320 K to help resolve peak overlap. All two-dimensional (2-D) spectra were acquired in the phase-sensitive mode using the states-time proportional phase increment (-TPPI) method (Marion et al. 1989) collecting $4{,}096(t_2) \times 1{,}024(t_1)$ data points with a sweep-width of 10 kHz and 48 scans per increment. Nuclear Overhauser effect spectroscopy (NOESY) spectra were acquired with mixing times of 20, 50, 70, and 150 ms (Brown et al. 1988; Jeener et al. 1979). Total correlation spectra were recorded using the clean total correlation spectroscopy (TOCSY) pulse sequence (Briand and Ernst 1991) with spin-lock times of 80 and 150 ms. Correlation spectroscopy (COSY) spectra were also acquired.

Data were processed using XWIN-NMR software (Bruker, Rheinstetten, Germany) with line narrowing of –5 Hz and gaussian broadening of 0.05 in the F_2 dimension, and by a cosine-squared function in the F_1 dimension. Polynomial baseline corrections were applied in both dimensions of each spectrum. Spectra were referenced to the chemical shift of water at each temperature (4.651 ppm at 308 K).

The software package XEASY (version 1.3.10) was used for assignment and integration of NOESY cross-peaks volumes. All nuclear Overhauser effects (NOEs) were measured in the 50-ms NOESY spectrum: the baseline around individual peaks (or peak clusters) was determined and used to correct peak volumes, and the volumes of NOESY cross-peaks for exchangeable protons were corrected for the percentage of $^{2}H_2O$ present.

Calculation of restraints

The NOESY cross-peak intensities were converted into upper and lower limit volumes (upv and lov, respectively) using the program INDYANA (Turner et al. 1999), which optimizes the scaling factors for converting NOE intensities into distances together with each structure. Interproton distances were taken to be proportional to the inverse fourth root of NOE intensities. Nonstereospecifically assigned protons, degenerate protons, overlapping peaks, and proline, phenylalanine, and tyrosine rings were treated as previously described (Brennan et al. 2000; Turner et al. 1999). The program GLOMSA (Guntert et al. 1991) was used to obtain stereospecific assignments.

Fixed upper and lower distance limits of 3.90 and 3.50 Å, respectively, were imposed between each pair of sulfur atoms involved in zinc coordination (C6, C9, C39, and C42). These distance constraints were based on the observed crys-

tallographic distances of the iron form (Sieker et al. 1994) and the observation that sulfur–zinc bond lengths are essentially identical to those of sulfur–iron bonds (Dauter et al. 1996). The range of distances allows a significant distortion of the tetrahedral geometry and does not specify the chirality of the center.

The distance restraints were used to generate protein conformers using the program DYANA, version 1.4, for restrained molecular dynamics with simulated annealing, with modifications (INDYANA) to optimize scaling factors for calibrating NOE intensities (Brennan et al. 2000). Annealing was performed using standard DYANA parameters with 20,000 steps.

In the final steps of structure refinement, the calculated structures were checked for interproton distances less than 3 Å for which no NOE had been measured. The volume at the predicted frequencies was measured and used in further calculations to ensure that the structures contain no short interproton distances in the absence of observable NOEs. A complete relaxation matrix analysis was applied to an ensemble of ten structures to estimate the error that might be introduced via spin-diffusion (Brennan et al. 2000). The root mean square deviation (rmsd) of the ratio between the theoretically corrected distance constraints and those determined by the automatic calibration in INDYANA was obtained for distances that exceeded the bounds set by INDYANA and used to loosen all the distance constraints in subsequent structure calculations.

Structure analysis

The program MOLMOL (Koradi et al. 1996), version 2.6, was used to superimpose and visualize the generated families of structures. The NMR structures were analyzed with respect to experimental constraints using standard procedures of the program DYANA. The quality of the structures with respect to dihedral angles was evaluated using the program PROCHECK-NMR, version 3.4.4 (Laskowski et al. 1996).

Secondary structural shifts were calculated for the ensemble of the 20 best structures using the program TOTAL (Williamson and Asakura 1993) and were compared with the difference between experimental values taken from the spectra and the average chemical shifts for each amino acid. Exchangeable protons were excluded from these calculations because of the possible influence of hydrogen bonding.

$^1H/^2H$ exchange experiments

Four NMR samples of rubredoxin (1 mM) were prepared in ^2H_2O containing 20 mM Tris-HCl (pH = 7.6). DGP (potassium salt), NaCl, or KCl were added to a final concentration of 100 mM in three of the samples. The sample tubes were kept at 90°C in a water bath and removed for short periods for acquisition of one-dimensional (1-D) ^1H-NMR spectra at 300 K (40 scans with a repetition delay of 2 s). The rate of proton/deuterium exchange of the amide protons was obtained from the dependence of the signal intensities on the time the sample had been kept at 90°C.

Protein data bank

The atomic coordinates were deposited in the Protein Data Bank at the Research Collaboratory for Structural Informatics with the accession code 1e8j.

Results

Signal assignment and spin-system identification

Sequence-specific ^1H-NMR assignments were accomplished using the classical approach (Wüthrich 1986). COSY and TOCSY spectra were acquired at different temperatures to identify spin systems, followed by sequence-specific assignment using NOESY spectra to identify sequential connectivities between the NH and H^α protons of different spin systems. The spin systems for Met-1 and Ser-22 could not be identified; this was probably due to the mobility of the N-terminus and the loop region around Ser-22, with consequent crowding of signals. Nevertheless, 83% of protons in this protein were assigned. The assignments are presented in Table 1.

Structure calculations

Assigned cross-peaks in the NOESY spectrum yielded 558 lovs and 700 upvs (Table 2). Analysis of preliminary structures using the program GLOMSA (Guntert et al. 1991) resulted in 34 stereospecific assignments derived from the stereo pairs with nondegenerate chemical shifts, and 74 NOEs (65%) that were pseudostereospecifically assigned to one or the other side of the fast-flipping aromatic side-chain rings. The effects of spin-diffusion were allowed for by setting a parameter in the program INDYANA to loosen all distance restraints by 5%. No torsion angle or hydrogen bond restraints were used. The experimental restraints were supplemented with fixed upper limits to represent covalent links in the flexible proline rings. The metal center was represented by a set of six upper and six lower fixed limits between the sulfur atoms of the four cysteines that coordinate the zinc atom.

A total of 500 random conformers were used as starting points for annealing by the INDYANA program. The 20 structures with the lowest target functions (from 0.47 $Å^2$ to 0.53 $Å^2$; average value, 0.51 $Å^2$, range, 12.7%) were selected as being representative of the solution structure of the protein. No consistent violations larger than 0.2 Å were found. The statistical analysis of violated restraints is given in Table 3.

The structures were superimposed using all heavy atoms (Fig. 1). The average rmsd value relative to the mean coordinates is 0.69 Å for the backbone atoms (N, C^α, and C′) and 1.09 Å for all heavy atoms (see Table 3). The calculated

Table 1. ^{1}H-NMR chemical shifts of *Desulfovibrio gigas* zinc rubredoxin at 35°C and pH 7.6

Residue	NH	Hα	Hβ	Other H
1 Met	–	–	–	
2 Asp	8.13	4.86	2.52; 2.82	
3 Ile	8.29	4.97	1.89	γCH^3 0.98; Hγ 1.42; δCH^3 1.05
4 Tyr	8.75	5.26	2.58; 2.79	Hδ(2,6) 6.74; H ∈ (3,5) 6.84
5 Val	9.44	5.32	2.08	γCH^3 1.00
6 Cys	9.62	3.04	3.08; 3.45	
7 Thr	8.53	4.35	3.97	γCH^3 1.54
8 Val	9.34	3.68	2.85	γCH^3(1) 1.01; γCH^3(2)1.02
9 Cys	9.29	5.25	2.75; 3.54	
10 Gly	8.19	3.94; 4.56		
11 Tyr	9.62	4.48	3.32; 3.52	Hδ(2,6) 7.61; H ∈ (3,5) 7.31
12 Glu	7.47	5.00	1.86; 2.01	Hγ 2.17; 2.62
13 Tyr	9.87	4.82	3.39; 3.40	Hδ(2,6) 7.41; H ∈ (3,5) 6.63; Hh(OH) 8.81
14 Asp	8.54	–	3.02; 3.29	
15 Pro		4.30	2.64	Hγ 1.67; Hδ 3.62; 3.70
16 Ala	8.42	4.23		βCH^3 1.55
17 Lys	7.88	4.58	2.20; 2.20	Hγ 1.64; 1.74; Hδ 2.02; 2.09; H ∈ 3.35
18 Gly	8.23	3.82; 4.09		
19 Asp	8.35	5.54	3.16; 3.37	
20 Pro		4.48	2.46	Hγ 2.14; Hδ 4.05; 4.34
21 Asp	8.21	4.41	1.10; 2.08	
22 Ser	–	–	–	
23 Gly	8.06	4.02; 4.43		
24 Ile	7.92	4.54	2.34	γCH^3 1.04; Hγ 1.48; 1.85; δCH^3 0.87
25 Lys	8.78	4.72	1.76; 1.92	Hγ 2.06
26 Pro		4.10	2.63; 3.22	–
27 Gly	9.17	3.67; 4.53		
28 Thr	7.46	4.47	4.08	γCH^3 1.19; Hγ(OH) 6.37
29 Lys	9.47	4.49	2.37	Hγ 2.03; Hδ 1.89; H ∈ 3.32
30 Phe	9.67	3.42	2.45; 2.86	Hδ(2,6) 6.26; H ∈ (3,5) 6.59; Hz 7.07
31 Glu	9.82	4.03	2.16; 2.29	Hγ 2.54; 2.62
32 Asp	7.61	4.88	2.73; 3.05	
33 Leu	7.24	4.04	0.51; 0.84	Hγ 1.00; δCH^3(1)-0.09; δCH^3(2)-1.51
34 Pro		4.40	2.13; 2.38	Hδ 3.46; 3.94
35 Asp	8.20	–	–	
36 Asp	8.42	4.82	–	
37 Trp	7.85	4.33	3.09; 3.17	Hδ1 7.39; Hz2 7.48; H ∈ 1 10.88; Hh2 7.14; H ∈ 3 6.84; Hz3 6.08
38 Ala	6.71	4.65		βCH^3 0.98
39 Cys	9.16	4.05	3.30; 3.37	
40 Pro		4.19	1.60; 2.13	Hγ 2.15; 2.48; Hδ 3.29; 3.69
41 Val	8.86	3.90	2.99	γCH^3(1) 1.07; γCH^3(2)1.09
42 Cys	8.96	5.16	2.77; 3.48	
43 Gly	8.16	3.95; 4.12		
44 Ala	9.37	4.43		βCH^3 1.70
45 Ser	8.35	4.84	4.36; 4.68	
46 Lys	8.97	4.48	2.19; 2.70	Hγ 1.40; 2.12; Hδ 1.57
47 Asp	8.54	5.40	2.60; 2.97	
48 Ala	8.61	–		βCH^3 1.82
49 Phe	8.40	5.62	2.78; 4.01	Hδ(2,6) 7.61; H ∈ (3,5) 7.79; Hz 7.93
50 Glu	9.26	5.08	2.07; 2.17	Hγ 2.54
51 Lys	8.78	3.62	1.46; 1.72	Hγ 1.05; Hδ 1.84; H ∈ 3.21
52 Gln	8.54	–	1.72; 1.82	–

structure presents a three-stranded antiparallel β-sheet, comprising residues 4–6, 12–13, and 49–51. There is also a hydrophobic core formed by the aromatic side chains of residues Tyr-4, Tyr-11, Tyr-13, Phe-30, Trp-37, and Phe-49, and a loop including residues 16 to 25 (see Fig. 1).

The four cysteines coordinate the metal ion in a tetrahedral geometry. The metal center is very well defined in the family of structures, with the heavy atoms of the cysteine residues having an rmsd smaller than 0.6 Å with respect to the mean structure. The chirality of the tetrahedrally bonded zinc center was not constrained; nevertheless, it is the same as that found in the X-ray structure of the iron form. A comparison between the crystal structure and the mean structure of the NMR ensemble shows an rmsd of all

Table 2. Number of restraints used for structure calculation

Distance restraints	Minimum volume limits (upper distance limits)	Maximum volume limits (lower distance limits)
Amino acid residues		
Intraresidual	176	190
Sequential (|i–j| = 1)	98	110
Medium range (2 = |i–j| < 5)	92	121
Long range (|i–j| = 5)	192	279
Total	558	700
Total nonredundant distance restraints	453	409
Nonredundant restraints per residue	17.95	

Table 3. Summary of scaling factors, restraint violations, and quality analysis

Quantity	Twenty conformers
A. Scaling factors[a]	
Proton–proton	41.4 ± 0.19
Proton–methyl	49.0 ± 0.41
Methyl–methyl	82.4 ± 1.14
Backbone proton–proton	42.1 ± 0.42
B. DYANA target function	
Average total (Å^2)	0.51 ± 0.014
Function range	0.47–0.53
C. Upper distance limit violations	
Average maximum (Å)	0.16 ± 0.02
No. of consistent violations (> 0.2 Å)	0
D. Lower distance limit violations	
Average maximum (Å)	0.23 ± 0.02
No. of consistent violations (> 0.2 Å)	0
E. Van der Waals violations	
Average maximum (Å)	0.18 ± 0.03
No. of consistent violations (> 0.2 Å)	0
F. Ramachandran plot (%)[b]	
Most favored	56.6 (64.7)
Additionally allowed	37.3 (34.3)
Generously allowed	5.4 (0.3)
Disallowed	0.8 (0.1)
G. Precision	
rmsd backbone (Å)	0.69 ± 0.10
rmsd heavy-atoms (Å)	1.09 ± 0.08

rmsd, root mean square deviation

[a] The scaling factor for each proton class (k) is defined by $k = r^4\sqrt{V}$, where r is the restrained interproton distance and V the NOE volume

[b] Percentages for residues with $S(\phi)$ and $S(\psi) > 0.8$ are shown in parentheses

heavy atoms of the cysteine residues of 0.56 Å and an rmsd of 0.21 Å in the sulfur atoms.

Several regions of the structure are well defined, with rmsd values smaller than 0.6 Å and angular order parameters for ϕ and ψ torsion angles larger than 0.80 (Fig. 2); this is the case for residues 3–9, 13–19, 24–33, and 36–51, which are mainly fragments that define the antiparallel β-sheet (present in all rubredoxins) and the hydrophobic core. Many of the remaining residues are located in the large hairpin loop and other exposed surface areas that tend to be poorly defined, with few NOE constraints per residue.

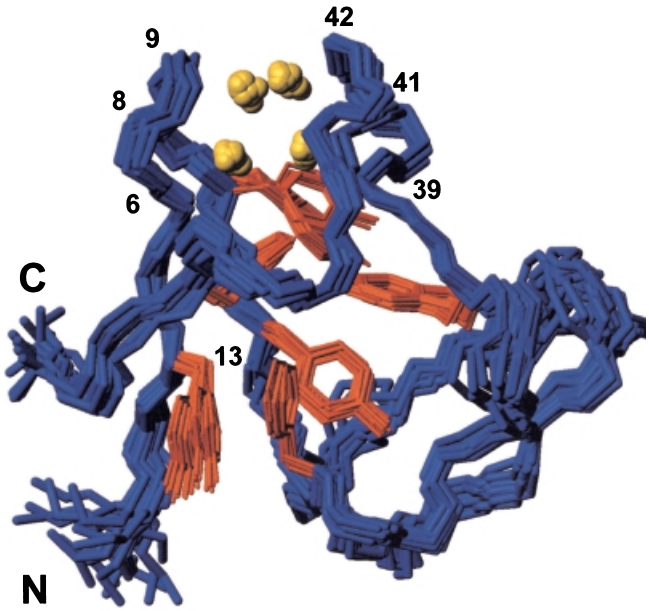

Fig. 1. Representation of the backbone (*blue*), aromatic side chains (*red*), and cysteine sulfur atoms (*yellow*) of the 20 best nuclear magnetic resonance (NMR) structures calculated for *Desulfovibrio gigas* rubredoxin. The *numbers* refer to the position of the residues displaying slow exchange rates of the amide groups

The deviation of the backbone torsion angles from ideality is represented by a Ramachandran plot (Ramachandran et al. 1963). The analysis made using the program PROCHECK-NMR (which only considers non-Gly, non-Pro, and nonterminal residues) showed that 56.6% of the residues are in the most favored region whereas only 0.8% are in disallowed regions (see Table 3). The residues falling in disallowed regions are Asp-21, Ser-22, Asp-35, and Lys-51, none of which is disallowed in more than 10% of the structures.

^{1}H/^{2}H amide exchange

The ^{1}H/^{2}H amide exchange rates in rubredoxin show a wide range of values. On ^2H_2O addition, several amide resonances became immediately undetectable in our experi-

mental conditions. At the lower end of the range, Cys-42 presented an exchange rate at 90°C of 1.55×10^{-4} s^{-1} (a half-life of 75 min). The method used here allowed the measurement of the exchange rates of the slowest exchanging amide protons, which belonged to Tyr-4, Val-5, Cys-6, Val-8, Cys-9, Gly-10, Tyr-13, Cys-39, Val-41, Cys-42, and Ala-44 (Fig. 3). The exchange rates of residues Tyr-4, Val-5, Gly-10, and Ala-44 were higher than 5×10^{-3} s^{-1}, and these values were excluded from Fig. 3 because of the large degree of uncertainty.

Using the program WHAT IF (Hooft et al. 1996), hydrogen bonds were found between the NH groups of Cys-6, Tyr-13, and Cys-39 to carbonyl groups (Table 4). Weaker hydrogen bonds to cysteine sulfurs were also found for the backbone amides of Val-8, Cys-9, Val-41, and Cys-42. On addition of DGP (potassium salt), exchange rates became slower. Furthermore, the decrease in rates when the solute was added was approximately proportional to the original rate (Fig. 3). To investigate the effect of the counterion, KCl was used at the same concentration as DGP and a small decrease of the exchange rates was observed, while NaCl produced a small increase in the rates (see Fig. 3).

Thermodynamic effect of the solutes

The mechanism of hydrogen exchange has been generally described by the following reaction scheme (Englander and Kallenbach 1984; Richarz et al. 1979):

$$\text{Closed} \underset{k_{cl}}{\overset{k_{op}}{\rightleftharpoons}} \text{Open} \xrightarrow{k_{ch}} \text{Exchanged}$$

With the exchange rate constant k_{ex} given by Eq. 1,

$$k_{ex} = k_{op}k_{ch}[Cat]/(k_{cl} + k_{ch}[Cat]) \quad (1)$$

where k_{op} is the rate constant for structural opening, k_{cl} is the rate constant for closing, k_{ch} is the rate constant for acid–base catalysis, and [Cat] is the catalyst concentration (Englander and Kallenbach 1984). In most examples of practical interest, the so-called EX2 condition prevails

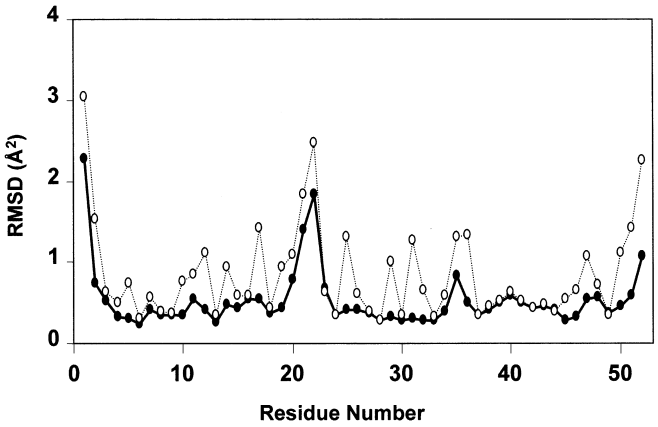

Fig. 2. Average backbone (*solid line*) and heavy atom (*dotted line*) root mean square deviation (rmsd) values per residue with respect to the mean structure of the NMR family. Structures were superimposed using all heavy atoms

Table 4. Optimal hydrogen bond network scores for *D. gigas* rubredoxin solution structure

Donor			Acceptor			Averaged score[a]
6	Cys	N	10	Gly	O	0.210
6	Cys	N	11	Tyr	O	0.059
8	Val	N	6	Cys	SG	0.178
9	Cys	N	9	Cys	SG	0.171
13	Tyr	N	4	Tyr	O	0.460
13	Tyr	N	11	Tyr	O	0.064
39	Cys	N	44	Ala	O	0.466
41	Val	N	39	Cys	SG	0.174
42	Cys	N	39	Cys	SG	0.187
42	Cys	N	42	Cys	SG	0.170

[a] Optimal hydrogen bond networks were calculated by the program WHAT IF (Vriend 1990) and the scores averaged over the 20 structures

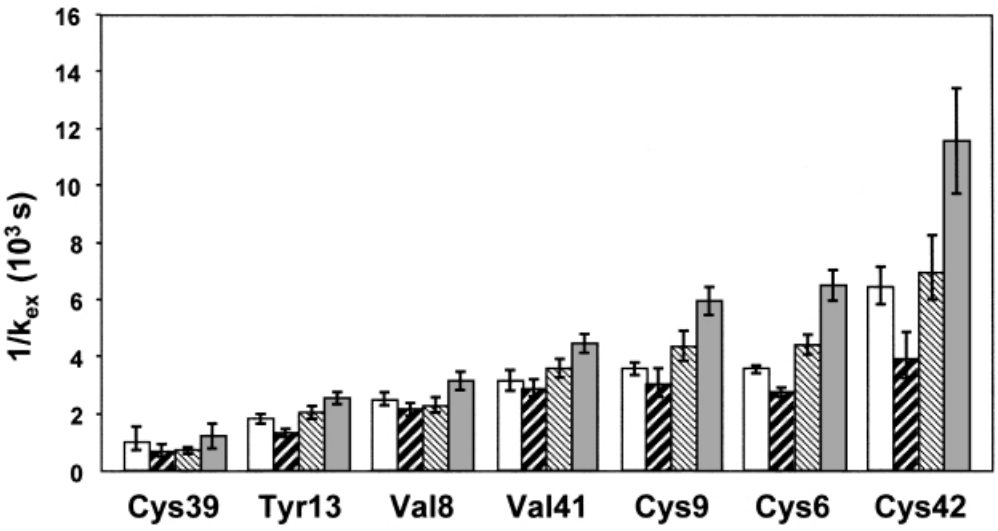

Fig. 3. Inverse of the proton exchange rates of the slower-exchanging amide protons in *Desulfovibrio gigas* rubredoxin measured at 90°C in the presence of 100 mM 1,1′-diglycerol phosphate (DGP) (*solid bars*), 100 mM KCl (*finely hatched bars*), 100 mM NaCl (*roughly hatched bars*), and no added solutes (*open bars*). *Error bars* represent three times the SD of the slope in semilog plots

(Englander and Mayne 1992; Hiller et al. 1997; Hvidt and Nielsen 1966; Roder et al. 1985; Wagner and Wüthrich 1979b); in this limiting situation, $k_{ch} << k_{cl}$, and Eq. 1 becomes

$$k_{ex} = K_{op}k_{ch}[Cat] \quad (2)$$

where $K_{op} = k_{op}/k_{cl}$ is the equilibrium constant for the structural opening that exposes the NH to exchange (Englander and Kallenbach 1984). Therefore, the structural stabilization free energy, ΔG, is given by $-RT\ n\ K_{op}$.

In the presence of a solute, the difference in the free energy change, ΔΔG, can be expressed by

$$\Delta\Delta G = RT \ln(k_{ex}/k_{ex}^{solute}) \quad (3)$$

where k_{ex}^{solute} is the rate constant in the presence of the solute. This expression holds whenever k_{ch} (rate of NH exchange in the open structure) is not altered by the solute.

The observed retardation of exchange of the rubredoxin amide protons shown in Fig. 3 in the presence of the solute DGP amounts to an additional structural stabilization of 1.2 ± 0.4 kJ/mol, with the uncertainty given as the standard deviation of the results. At the same concentration, KCl provided a stabilization of 0.1 ± 0.5 kJ/mol, whereas NaCl showed a destabilization of 0.7 ± 0.3 kJ/mol.

Discussion

NMR solution structure

The NMR structure of *D. gigas* zinc rubredoxin in solution presents the same overall features as the iron form (Sieker et al. 1994). Both forms contain a three-stranded β-sheet, an exposed hairpin loop on the opposite side of the protein, the hydrophobic core formed by the side chains of six residues, and the metal center coordinated by four cysteines. The comparison between the NMR (Zn-form) and crystal (Fe-form) structures clearly shows that zinc substitution does not alter the protein structure significantly: the rmsd between the backbones of the crystal structure and the mean NMR structure is 1.12 Å, and the pattern of hydrogen bonds is similar. These results are in agreement with results for other rubredoxins, in which Zn substitution leaves the structure virtually unchanged while avoiding the difficulties that arise from the paramagnetism of the iron center (Blake et al. 1992; Dauter et al. 1996).

The calculated chemical shifts for the NMR ensemble were compared with the observed shifts to confirm assignments and to evaluate the agreement between the structures and the experimental data. The plots of experimental versus observed ring current shifts for the NMR ensemble (average over 20 conformers) and for the crystal structure are shown in Fig. 4. These plots show that both the NMR and the X-ray structures give fits of similar quality.

$^1H/^2H$ amide exchange

With the exception of Tyr-4 and Tyr-13 (involved in hydrogen bonding in the β-sheet), the slow amide proton exchange rates are all clustered around the metal center (Fig. 1). A similar pattern of exchange was observed in the rubredoxin from *Pyrococcus furiosus* (Hiller et al. 1997). Rubredoxin is a small protein in which virtually all the backbone is exposed to the solvent. As a consequence, fast amide proton exchange rates are expected for all residues not involved in hydrogen bonds, and the fast time scale for the exchange rates of many amide protons elegantly measured in the hyperthermostable rubredoxin from *P. furiosus* may be not too surprising (Hernandez et al. 2000).

On closer inspection of the solution structure of *D. gigas* rubredoxin, we observe that the amide protons surrounding the metal center are all pointing inward and relatively shielded from solvent access, whereas the rest of the amides are in contact with the solvent. The slow-exchanging amide protons around the metal center are involved in rather weak hydrogen bonds (see Table 4); hence, the reason for the observed slow exchange rates must involve restricted local solvent access despite the small size of this protein. Therefore, the exchange rates of these slowly exchanging

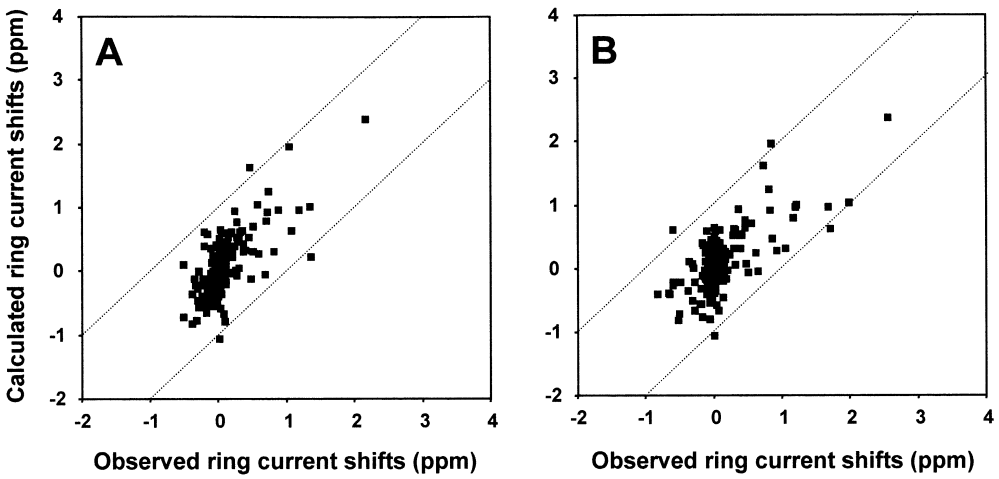

Fig. 4. Observed ring current shifts for each unique or stereo assigned proton versus (**A**) average calculated ring current shifts for the 20 best conformers of the NMR ensemble and (**B**) calculated ring current shifts for the crystal structure of *Desulfovibrio gigas* (Fe)-rubredoxin

residues are appropriate probes to monitor global protein stability (Englander et al. 1996; Wagner and Wüthrich 1979a).

DGP caused a considerable retardation of the exchange of slowly exchanging amide protons, measured at physiological pH, which demonstrates the stabilizing effect of this solute on the structure of rubredoxin. The decrease in exchange rates (see Fig. 3) exhibits an approximate proportionality that implies a common mechanism and suggests that these amide protons all exchange in the same locally unfolded state. According to Cavagnero et al. (1998), metal loss is one of the early steps in the rubredoxin unfolding reaction without which subsequent steps do not take place. The demonstrated ability of DGP to stabilize the local metal-binding structure could explain the enhancement of protein stability. It is interesting to note that Tyr-13, part of the β-sheet, behaves in a fashion similar to residues closer to the metal center, suggesting that the β-sheet is involved in the local unfolding.

The use of Eq. 3 to calculate changes in the stabilization energy assumes that the rate of exchange of the amides in the open structure is unaltered by the solutes (Foord and Leatherbarrow 1998). The metal center is negatively charged and the carbonyl groups of the surrounding residues point outward, creating an electrostatic barrier to catalysis by OH^-. In this context, the presence of a charged solute increasing the ionic strength of the solvent could make a significant difference to k_{ch} values. However, our control measurements of the exchange rates in the presence of NaCl and KCl at the same ionic strength showed that ionic strength alone does not account for the retardation effects observed with DGP.

The stability of *D. gigas* rubredoxin is increased by 1.2 kJ/mol in 100 mM DGP. Larger effects have been observed using other solute–protein systems. For instance, 2 M glycine produced an enhancement of 17.3 kJ/mol in the stability of horse heart cytochrome *c* and 7.7 kJ/mol for chymotrypsin inhibitor 2 (Foord and Leatherbarrow 1998). The stability of ribonuclease A was increased by 30.2 kJ/mol by the addition of 8.2 M sarcosine (Santoro et al. 1992) and 10.6 kJ/mol by 3 M β-hydroxyectoine (Knapp et al. 1999). The stabilizing effect of a given solute is dependent on the protein chosen. However the effect is often approximately linear in the solute concentration. Thus, the effectiveness of DGP in stabilizing *D. gigas* rubredoxin compares favorably with the effects found in other systems.

DGP has proven to have a strong stabilizing effect on several enzymes and iron rubredoxins from different sources (Lamosa et al. 2000), and this has now also been demonstrated in the zinc form of *D. gigas* rubredoxin using NMR. The presence of DGP, KCl, and NaCl left the spectra of rubredoxin virtually unchanged. As ^{1}H-NMR chemical shifts are a sensitive probe of protein conformation, this fact is consistent with the maintenance of the protein structure. Thus, stabilization by DGP does not involve changes in the protein structure. Because the more rapid amide exchange rates in rubredoxin appear to reflect the dynamics of individual hydrogen bonds (Hernandez et al. 2000), we conclude that concerted movements around the metal center and in the β-sheet reflect the global stability of the protein.

The availability of tailored mutants of *D. gigas* rubredoxin and of DGP specifically enriched with carbon-13 provides us with an excellent model system for using NMR to investigate mechanisms of protein thermostabilization by compatible solutes.

Acknowledgments This work was supported by PRAXIS XXI and FEDER, Portugal (PRAXIS/BIO/12082/98 to H.S.) and by TMR contract number ERBFMRX-CT98-0218. P. Lamosa acknowledges a Ph.D. grant from PRAXIS XXI (BD/11474/97).

References

Arakawa T, Timasheff SN (1985) The stabilization of proteins by osmolytes. Biophys J 47:411–414

Arakawa T, Bhat R, Timasheff SN (1990) Why preferential hydration does not always stabilize the native structure of globular proteins. Biochemistry 29:1924–1931

Blake PR, Day MW, Hsu BT, Joshua-Tor L, Park JB, Hare DR, Adams MW, Rees DC, Summers MF (1992) Comparison of the X-ray structure of native rubredoxin from *Pyrococcus furiosus* with the NMR structure of the zinc-substituted protein. Protein Sci 1:1522–1525

Brennan L, Turner DL, Messias AC, Teodoro ML, LeGall J, Santos H, Xavier AV (2000) Structural basis for the network of functional cooperativities in cytochrome c(3) from *Desulfovibrio gigas*: solution structures of the oxidised and reduced states. J Mol Biol 298:61–82

Briand J, Ernst RR (1991) Computer-optimized homonuclear TOCSY experiments with suppression of cross-relaxation. Chem Phys Lett 185:276–285

Britton KL, Baker PJ, Borges KM, Engel PC, Pasquo A, Rice DW, Robb FT, Scandurra R, Stillman TJ, Yip KS (1995) Insights into thermal stability from a comparison of the glutamate dehydrogenases from *Pyrococcus furiosus* and *Thermococcus litoralis*. Eur J Biochem 229:688–695

Britton KL, Yip KS, Sedelnikova SE, Stillman TJ, Adams MW, Ma K, Maeder DL, Robb FT, Tolliday N, Vetriani C, Rice DW, Baker PJ (1999) Structure determination of the glutamate dehydrogenase from the hyperthermophile *Thermococcus litoralis* and its comparison with that from *Pyrococcus furiosus*. J Mol Biol 293:1121–1132

Brown SC, Weber PL, Mueller L (1988) Towards complete ^{1}H NMR spectra in proteins. J Magn Reson 77:166–169

Cavagnero S, Zhou ZH, Adams MW, Chan SI (1998) Unfolding mechanism of rubredoxin from *Pyrococcus furiosus*. Biochemistry 37:3377–3385

da Costa MS, Santos H, Galinski EA (1998) An overview of the role and diversity of compatible solutes in Bacteria and Archaea. Adv Biochem Eng Biotechnol 61:117–153

Dauter Z, Wilson KS, Sieker LC, Moulis JM, Meyer J (1996) Zinc- and iron-rubredoxins from *Clostridium pasteurianum* at atomic resolution: a high-precision model of a ZnS_4 coordination unit in a protein. Proc Natl Acad Sci USA 93:8836–8840

Englander SW, Kallenbach NR (1984) Hydrogen exchange and structural dynamics of proteins and nucleic acids. Q Rev Biophys 16:521–655

Englander SW, Mayne L (1992) Protein folding studied using hydrogen-exchange labeling and two-dimensional NMR. Annu Rev Biophys Biomol Struct 21:243–265

Englander SW, Sosnick TR, Englander JJ, Mayne L (1996) Mechanisms and uses of hydrogen exchange. Curr Opin Struct Biol 6:18–23

Felix CF, Moreira CC, Oliveira MS, Sola-Penna M, Meyer-Fernandes JR, Scofano HM, Ferreira-Pereira A (1999) Protection against thermal denaturation by trehalose on the plasma membrane H^+-ATPase from yeast. Synergetic effect between trehalose and phospholipid environment. Eur J Biochem 266:660–664

Foord RL, Leatherbarrow RJ (1998) Effect of osmolytes on the exchange rates of backbone amide protons in proteins. Biochemistry 37:2969–2978

Guntert P, Braun W, Wüthrich K (1991) Efficient computation of three-dimensional protein structures in solution from nuclear magnetic resonance data using the program DIANA and the supporting programs CALIBA, HABAS and GLOMSA. J Mol Biol 217:517–530

Hensel R (1993) Proteins of extreme thermophiles. New Comp Biochem 26:209–221

Hensel R, König H (1988) Thermoadaptation of methanogenic bacteria by intracellular ion concentration. FEMS Microbiol Lett 49:75–79

Hernandez G, Jenney FE Jr, Adams MW, LeMaster DM (2000) Millisecond time scale conformational flexibility in a hyperthermophile protein at ambient temperature. Proc Natl Acad Sci USA 97:3166–3170

Hiller R, Zhou ZH, Adams MW, Englander SW (1997) Stability and dynamics in a hyperthermophilic protein with melting temperature close to 200 degrees C. Proc Natl Acad Sci USA 94:11329–11332

Hooft RWW, Sander C, Vriend G (1996) Positioning hydrogen atoms by optimizing hydrogen-bond networks in protein structures. Proteins 26:363–376

Hvidt A, Nielsen SO (1966) Hydrogen exchange in proteins. Adv Protein Chem 21:287–386

Jaenicke R (1991) Protein stability and molecular adaptation to extreme conditions. Eur J Biochem 202:715–728

Jaenicke R, Bohm G (1998) The stability of proteins in extreme environments. Curr Opin Struct Biol 8:738–748

Jeener J, Meier BH, Bachmann P, Ernst RR (1979) Investigation of exchange processes by two-dimensional n.m.r. spectroscopy. J Chem Phys 71:4546–4553

Karshikoff A, Ladenstein R (1998) Proteins from thermophilic and mesophilic organisms essentially do not differ in packing. Protein Eng 11:867–872

Knapp S, Ladenstein R, Galinski EA (1999) Extrinsic protein stabilization by the naturally occurring osmolytes beta-hydroxyectoine and betaine. Extremophiles 3:191–198

Koradi R, Billeter M, Wüthrich K (1996) MOLMOL: a program for display and analysis of macromolecular structures. J Mol Graph 14:51–55

Ladenstein R, Antranikian G (1998) Proteins from hyperthermophiles: stability and enzymatic catalysis close to the boiling point of water. Adv Biochem Eng Biotechnol 61:37–85

Lamosa P, Burke A, Peist R, Huber R, Liu MY, Silva G, Rodrigues-Pousada C, LeGall J, Maycock C, Santos H (2000) Thermostabilization of proteins by diglycerol phosphate, a new compatible solute from the hyperthermophile *Archaeoglobus fulgidus*. Appl Environ Microbiol 66:1974–1979

Laskowski RA, Rullmannn JA, MacArthur MW, Kaptein R, Thornton JM (1996) AQUA and PROCHECK-NMR: programs for checking the quality of protein structures solved by NMR. J Biomol NMR 8:477–486

Lebbink JH, Knapp S, van der Oost J, Rice D, Ladenstein R, de Vos WM (1999) Engineering activity and stability of *Thermotoga maritima* glutamate dehydrogenase. II: Construction of a 16-residue ion-pair network at the subunit interface. J Mol Biol 289:357–369

Lippert K, Galinski EA (1992) Enzyme stabilization by ectoine-type compatible solutes: protection against heating, freezing and drying. Appl Microbiol Biotechnol 37:61–65

Marion D, Ikura M, Tschudin R, Bax A (1989) Rapid recording of 2D NMR spectra without phase cycling. Application to the study of hydrogen exchange in proteins. J Magn Reson 85:393–399

Martins LO, Huber R, Huber H, Stetter KO, da Costa MS, Santos H (1997) Organic solutes in hyperthermophilic Archaea. Appl Environ Microbiol 63:896–902

Perl D, Mueller U, Heinemann U, Schmid FX (2000) Two exposed amino acid residues confer thermostability on a cold shock protein. Nat Struct Biol 7:380–383

Ramachandran G, Ramakrishnan C, Sasisekharan V (1963) Stereochemistry of polypeptide chain configurations. J Mol Biol 7:95–99

Ramos A, Raven NDH, Sharp RJ, Bartolucci S, Rossi M, Cannio R, Lebbink J, van der Oost J, de Vos WM, Santos H (1997) Stabilization of enzymes against thermal stress and freeze-drying by mannosylglycerate. Appl Environ Microbiol 63:4020–4025

Richards FM (1997) Protein stability: still an unsolved problem. Cell Mol Life Sci 53:790–802

Richarz R, Sehr P, Wagner G, Wüthrich K (1979) Kinetics of the exchange of individual amide protons in the basic pancreatic trypsin inhibitor. J Mol Biol 130:19–30

Roder H, Wagner G, Wüthrich K (1985) Amide proton exchange in proteins by EX1 kinetics: studies of the basic pancreatic trypsin inhibitor at variable p^2H and temperature. Biochemistry 24:7396–7407

Santoro MM, Liu Y, Khan SM, Hou LX, Bolen DW (1992) Increased thermal stability of proteins in the presence of naturally occurring osmolytes. Biochemistry 31:5278–5283

Santos H, da Costa MS (2001) Organic solutes from thermophiles and hyperthermophiles. Methods Enzymol 336: 302–315

Scholz S, Sonnenbichler J, Schäfer W, Hensel R (1992) Di-*myo*-inositol-1,1′-phosphate: a new inositol phosphate isolated from *Pyrococcus woesei*. FEBS Lett 306:239–242

Shima S, Tziatzios C, Schubert D, Fukada H, Takahashi K, Ermler U, Thauer RK (1998) Lyotropic-salt-induced changes in monomer/dimer/tetramer association equilibrium of formyltransferase from the hyperthermophilic *Methanopyrus kandleri* in relation to the activity and thermostability of the enzyme. Eur J Biochem 258:85–92

Sieker LC, Stenkamp RE, LeGall J (1994) Rubredoxin in crystalline state. Methods Enzymol 243:203–216

Strop P, Mayo SL (2000) Contribution of surface salt bridges to protein stability. Biochemistry 39:1251–1255

Timasheff SN (1993) The control of protein stability and association by weak interactions with water: how do solvents affect these processes? Annu Rev Biophys Biomol Struct 22:67–97

Turner DL, Brennan L, Meyer HE, Lohaus C, Siethoff C, Costa HS, Gonzalez B, Santos H, Suarez JE (1999) Solution structure of plantaricin C, a novel lantibiotic. Eur J Biochem 264:833–839

Vriend G (1990) WHAT IF: a molecular model and drug design program. J Mol Graph 8:52–56

Wagner G, Wüthrich K (1979a) Correlation between the amide proton exchange rates and the denaturation temperatures in globular proteins related to the basic pancreatic trypsin inhibitor. J Mol Biol 130:31–37

Wagner G, Wüthrich K (1979b) Structural interpretation of the amide proton exchange in the basic pancreatic trypsin inhibitor and related proteins. J Mol Biol 134:75–94

Williamson MP, Asakura T (1993) Empirical comparisons of models for chemical shift calculations in proteins. J Magn Reson Ser B 101:63–71

Wüthrich K (1986) NMR of proteins and nucleic acids. Wiley, New York